

Effect of Pump and Probe Light Field on Picosecond Time-Resolved Resonance Raman Spectra of S_1 *trans*-Stilbene. Disagreement between Stokes- and Anti-Stokes Scattering Frequencies

Koichi Iwata

Research Centre for Spectrochemistry, School of Science, The University of Tokyo,
3-2-1 Hongo, Bunkyo-ku, Tokyo 113-0033

(Received October 9, 2001)

Picosecond time-resolved spontaneous resonance Raman spectra of the first excited singlet (S_1) state of *trans*-stilbene were measured with various power densities of pump or probe light, for both the Stokes and anti-Stokes scattering regions. Careful calibration of the peak positions of the 285 cm^{-1} Raman bands reveals that the Stokes scattering band and the anti-Stokes scattering band shift to the same direction in absolute wavenumber, or to the opposite directions in Raman shift, when the pump or probe power density is increased. The direction of the wavenumber shift caused by the pump light field is opposite to that caused by the probe. Because of these apparent peak shifts, the Stokes Raman band and the anti-Stokes Raman band are recorded at different Raman shifts. The intrinsic change of the vibrational level spacing and the apparent peak shift caused by the pump or probe light field can be clearly separated by calculating the "symmetric" and "anti-symmetric" components from the Stokes and anti-Stokes peak positions. The experimental results are not explained by the optical Stark effect in its simplest form. Possible mechanisms to account for the results are discussed.

The presence of a strong light field affects optical processes in various types of spectroscopy. The effect of the strong light field on steady state optical absorption and emission processes in a two-level system has been well formulated as the optical Stark effect.[1,2] In time-resolved spectroscopy, the deformation of the absorption band caused by strong "pump" light field in a "pump–probe" experiment has been explained well by the optical Stark effect.[3] In Raman spectroscopy, the broadening or peak shift of Raman bands under strong "probe" light field has been explained by lifetime shortening of the initial state by optical depletion[4] or by a non-perturbative approach in which the time evolution of the density operator is estimated by solving the Liouville equation.[5,6] Picosecond time-resolved spontaneous resonance Raman spectra of the first excited singlet (S_1) state of *p*-terphenyl demonstrated that the position and the width of its Raman band were changed by the pump light field.[7] The dependence of the pump light field on time-resolved spontaneous Raman spectra, however, has not yet been thoroughly examined. Nor has the effect of strong light fields on the anti-Stokes scattering Raman bands been clarified.

The S_1 state of *trans*-stilbene is a precursor of the *trans–cis* isomerization reaction, a well-studied unimolecular reaction that can be triggered by photoexcitation.[8,9] It is one of molecular species studied most thoroughly with time-resolved Raman spectroscopy.[10,11] Many of its Raman bands have been assigned based on the observed spectral shifts on isotope substitutions.[12] It has been established that its Stokes peak positions and bandwidths change depending on the probe laser power,[13] time delay between the pump and probe pulses,[14–16] or temperature of the bulk[16,17] or micellar[18] solutions. Anti-Stokes scattering bands in the low wavenumber region[17] as well as the finger print region[19–23] have been detected, although the reason for the large enhancement for the anti-Stokes finger print region remains puzzling. It is ideal to use S_1 *trans*-stilbene when studying a new phenomenon observed with picosecond time-resolved Raman spectroscopy.

Intensities of anti-Stokes Raman scattering bands have been utilized to probe the dynamics of population change in vibrational levels.[17,19–25] We used the intensity of the 285 cm^{-1} band of S_1 *trans*-stilbene for tracing the vibrational cooling kinetics,[17] together with the position of the 1570 cm^{-1} band. In the course of this study, we noticed that the peak position of the 285 cm^{-1} band changed depending on the pump or probe power intensities and that the direction of the peak shift for the Stokes and anti-Stokes scattering bands was not easily explained.

The peak position of a Raman band contains rich information on the structure and dynamics of a studied molecule. Picosecond time-resolved Raman spectra of the S_1 state of *trans*-stilbene have revealed that the position of the C=C stretch vibration band at 1570 cm^{-1} can be used as a "picosecond Raman thermometer".[17] The newly obtained thermometer made it possible to study the excess energy dissipation process from S_1 *trans*-stilbene in detail and to establish a simple numerical model to account for the process. For this study, determination of the peak position with a precision better than 1 cm^{-1} was required. Reliable determination of the positions of Raman bands is crucial when trying to extract maximum information from a recorded set of Raman spectra.

In this article, we report the pump and probe power depen-

dence of the Stokes and anti-Stokes Raman scattering of S_1 *trans*-stilbene. As the power of the pump or probe light increases, positions of the Stokes and anti-Stokes scattering bands move to the same direction in absolute wavenumber, or to the opposite directions in Raman shift. Possible mechanisms that explain this unexpected event are discussed.

Experimental

The details of our picosecond time-resolved Raman spectrometer has been described elsewhere.[26] In short, output from a mode-locked dye laser (Spectra Physics 3520), synchronously pumped by a cw mode-locked Nd:YAG laser (Spectra Physics 3800S), was amplified by a cw Nd:YAG regenerative amplifier (Spectra Physics 3800RA). The output from the amplifier (588 nm, 2 kHz) was frequency-doubled by a BBO crystal. The obtained second harmonic (294 nm, 1–2 mW) was used as pump light. The remaining fundamental (588 nm) was used as probe. The amplified probe light pulse was close to the Fourier transform limit (see below).

The light scattered from the sample to the 90 degree direction was collected with a pair of lenses, focused onto the entrance slit of a single spectrograph (Instruments SA HR320), and detected with a liquid-nitrogen-cooled CCD detector (Princeton Instruments LN/CCD-1024 TKB). A holographic notch filter centered at 588 nm (Kaiser Optical Systems) was placed in front of the entrance slit of the spectrograph to eliminate the elastic scattering component.

By using a CCD detector, two-dimensional images at the focal plane of the spectrograph were easily obtained. Each Raman signal appeared as a vertical image of the entrance slit, while the fluorescence from the sample formed a horizontal band, whose vertical length corresponded to the penetration depth of the pump light. The condition for the pixel binning of the CCD image was determined so that the scattering signals were collected only from the area where fluorescence was observed, that is, where the S_1 state of *trans*-stilbene was present. Scattering from other parts of the sample would contribute only to the solvent Raman bands.

The sample solution was circulated through a dye laser nozzle. The pump and probe laser pulses were focused on a flat surface of the sample solution formed after the nozzle. Beam diameters for the pump and probe light were measured by moving a razor blade on a translational stage at the sampling point. Fitting the error function to the recorded profiles of the transmitted light intensity gave the beam diameter (FWHM) of 110 μm for the pump beam and 40 μm for the probe.

Results and Discussion

Pump and Probe Power Dependence of the Stokes and Anti-Stokes Scattering Bands. In this article, we concentrate mostly on the 285 cm^{-1} band of S_1 *trans*-stilbene, because it is one of the two anti-Stokes Raman bands we detect. The other band located at 200 cm^{-1} has a smaller intensity.[17,27] Internal standard bands from the solvent, for calibrating the position or intensity of the solute bands, are available in this spectral region. Both the Stokes and anti-Stokes bands, as well as the Rayleigh band, can be recorded in a single exposure with a sufficient wavenumber resolution. An example of a set of time-resolved spectra of S_1 *trans*-stilbene in chloroform is shown in Fig. 1. In the figure, panel (A) and panel (B) show the Stokes scattering side and the anti-Stokes scattering side.

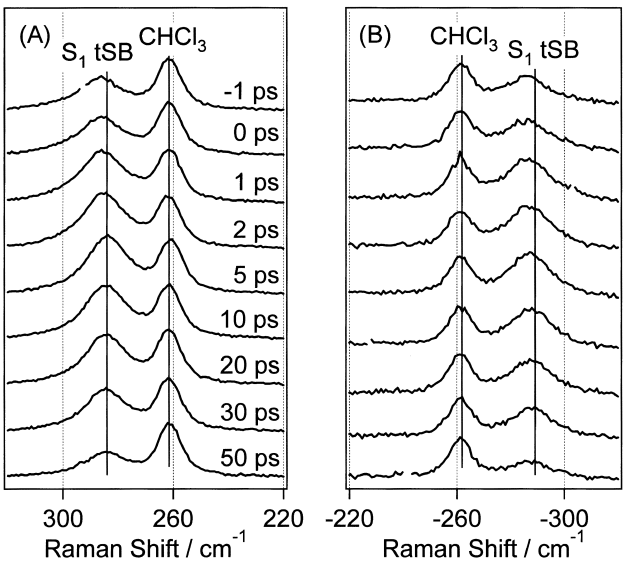

Fig. 1. Time-resolved Raman spectra of S_1 *trans*-stilbene in chloroform. Stokes scattering bands (A) and anti-Stokes scattering bands (B). Raman bands from S_1 *trans*-stilbene and solvent chloroform as well as time delay for each spectrum are indicated in the figure.

Raman bands at 285 cm^{-1} and 261 cm^{-1} are assigned to S_1 *trans*-stilbene and solvent chloroform, as indicated in the figure.

We selected chloroform as the solvent because we can use its 261 cm^{-1} band, located close to the 285 cm^{-1} band of S_1 *trans*-stilbene, as a good internal standard. It should be noted that the probe light of 588 nm is in strong resonance with the S_n–S_1 transition of *trans*-stilbene,[8] but not in resonance with transitions of chloroform.

In Fig. 1, the 285 cm^{-1} band from S_1 *trans*-stilbene changes its position depending on the time after the photoexcitation, while the 261 cm^{-1} band from chloroform does not change its position. This phenomenon is similar to the time dependent wavenumber shift observed for some Raman bands in the finger print region.[14–16] However, the direction of the wavenumber shift shown in Fig. 1 is totally unexpected. In the figure, the Stokes band at 285 cm^{-1} moves to the lower wavenumber direction in Raman shift, approaching the Rayleigh line, as the time delay increases. On the contrary, the anti-Stokes band for the same vibrational mode moves to the opposite direction, shifting away from the Rayleigh line, for the same period of time. In ordinary cases, the Raman shift values for a Stokes scattering band and the corresponding anti-Stokes scattering band from the same vibrational mode are always equal. Even if they change their positions as the time delay increases, we expect them to keep the same Raman shift values.

A schematic diagram illustrating the observed time dependence of the Raman bands from S_1 *trans*-stilbene and chloroform is shown in Fig. 2. A vertical arrow at the center of the figure, from the top to the bottom, indicates the increase of time delay between the pump and probe. Horizontal axis (not shown) represents the energy of light. The energy of light becomes larger at the right-hand side of the figure. Peak positions of the solute and solvent bands are represented by solid

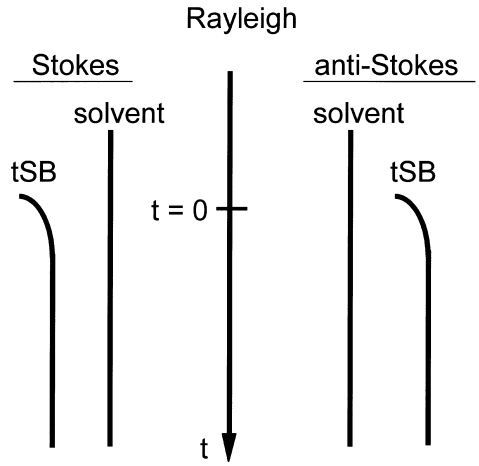

Fig. 2. Schematic diagram showing the time dependence of Raman bands from S_1 *trans*-stilbene and solvent chloroform. The Stokes scattering bands are shown in the left half while the anti-Stokes scattering bands are in the right half.

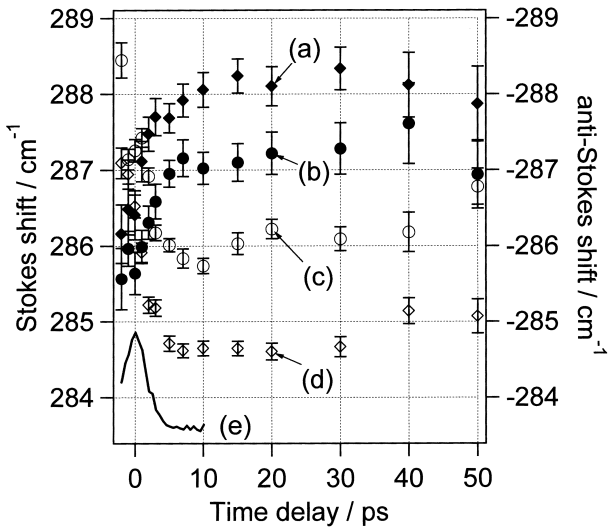

Fig. 3. Time dependence of the peak positions of the 285 cm^{-1} Raman band of S_1 *trans*-stilbene measured in chloroform. Anti-Stokes scattering band with the probe power density of 31 GW cm^{-2} (a), anti-Stokes with 7.4 GW cm^{-2} (b), Stokes scattering band with the probe power density of 7.4 GW cm^{-2} (c), and Stokes with 31 GW cm^{-2} (d).

traces. The figure shows that the "apparent excitation energy" of the probe light changes as the time delay evolves only for the S_1 *trans*-stilbene bands. The experimental result that the Stokes and anti-Stokes scattering Raman bands of S_1 *trans*-stilbene move to the same direction in absolute light energy might seem quite strange. It is not explained, however, by a simple error in wavenumber calibration. The Stokes and anti-Stokes scattering bands from chloroform were recorded at the same positions throughout the measurement.

For further analysis of the experimental data, positions of the observed Raman bands were calculated by fitting the Lorentzian function to the recorded Raman bands. The obtained peak position is plotted against the time delay in Fig. 3. In the figure, filled markers (a and b) indicate the anti-Stokes scattering Raman bands while open markers (c and d) show the Stokes counterparts. Two sets of data were measured under the probe power densities of 31 GW cm^{-2} (a and d) and 7.4 GW cm^{-2} (b and c).

It is obvious from the figure that the Stokes Raman band and the anti-Stokes Raman band change their positions depending on the time delay. For the time region between 0 ps and 5 ps, a steep decrease in Raman shift is observed for the Stokes scattering Raman band, while a mirror image increase in Raman shift is observed for the anti-Stokes scattering band. As illustrated in Fig. 2, the Stokes scattering band and the anti-Stokes scattering band move to the opposite directions in Raman shift. They reach stationary positions after 10 ps. One might claim that this peak shift reflects the cooling process of S_1 *trans*-stilbene, because it has been established that the cooling process causes a similar wavenumber shift in the Stokes side.[17] This possibility is denied, however, because the time constant for the cooling process in chloroform was measured to be 12 ps (see Fig. 7), much slower than the kinetics observed in Fig. 3. It should be noted that the kinetics of the positional change of the 1570 cm^{-1} agrees with the anti-Stokes/Stokes intensity change of the 285 cm^{-1} band.[17]

The observed time dependence of the Stokes and anti-Stokes peak positions is quite similar to the cross correlation function between the pump pulse and the probe pulse obtained by difference frequency mixing of the two pulses (Fig. 3(e)). This agreement suggests that the Stokes and anti-Stokes peak shifts between 0 ps and 5 ps are caused by the presence of the pump light field.

There is another unexpected observation in Fig. 3, besides the direction of the time dependent peak shift. Although the Stokes and anti-Stokes Raman bands reach the stationary positions after 10 ps, these Raman shift values are different from each other. With the probe power density of 7.4 GW cm^{-2}, for example, the Stokes band is located at around 286 cm^{-1} while the anti-Stokes band is at 287 cm^{-1}. For the probe power density of 31 GW cm^{-2}, the discrepancy is even larger. As mentioned above, however, the Stokes and anti-Stokes scattering Raman bands from the 261 cm^{-1} vibrational mode of chloroform appear at exactly the same position. The probe light field, as well as the pump light field, affects only the peak position of the Raman bands of S_1 *trans*-stilbene, but not the solvent Raman bands.

For clarifying the effect of the probe light field further, we measured the Raman spectrum of S_1 *trans*-stilbene with various probe power densities at a fixed time delay. The results for the 285 cm^{-1} bands are shown in Fig. 4. The time delay was set to be 50 ps, when the vibrational cooling process of photoexcited S_1 *trans*-stilbene was completed. In the figure, small dots represent obtained data points, while the best fit Lorentzian functions are shown with solid curves. As the probe power density increased from 2.9 GW cm^{-2} (c) to 31 GW cm^{-2} (a), the peak position of the Stokes scattering band moves downward to the lower wavenumber direction. The corresponding anti-Stokes scattering band, on the contrary, moves upward to the higher wavenumber direction during the course of the probe power increase.

The width of the Stokes or anti-Stokes scattering Raman

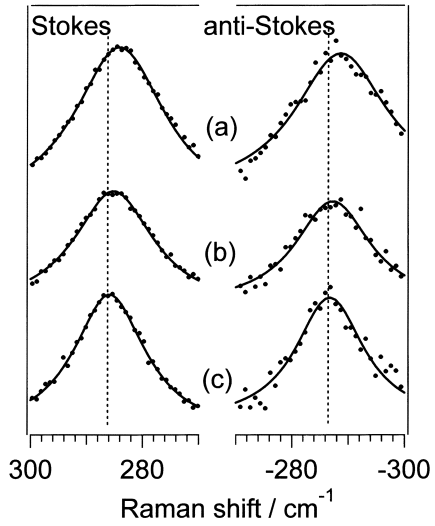

Fig. 4. Probe power dependence of the Stokes and anti-Stokes Raman bands of S_1 *trans*-stilbene. Spectral areas for the 285 cm^{-1} band are shown. The spectrum was measured in chloroform with the probe power density of 31 GW cm^{-2} (a), 10 GW cm^{-2} (b), and 2.9 GW cm^{-2} (c).

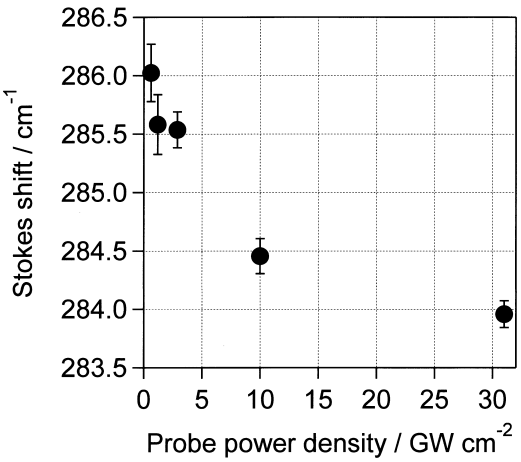

Fig. 5. Dependence of peak position of the 285 cm^{-1} Stokes Raman band of S_1 *trans*-stilbene in chloroform on probe power density. The time delay was set at 50 ps.

band also shows probe power dependence. The width increases when the probe power is increased. There is no significant difference detected on the band broadening between the Stokes scattering band and the anti-Stokes scattering band.

The peak position of the 285 cm^{-1} Stokes Raman scattering band measured at 50 ps is plotted against the probe power density in Fig. 5. The peak position was calculated by fitting the Lorentzian function to the observed Raman band, as demonstrated in Fig. 4. The observed peak position is clearly affected by the probe light field. When the probe power density is changed from 0.62 to 31 GW cm^{-2}, the peak position of the Stokes scattering band changes by 2 cm^{-1}, from 286.0 to 284.0 cm^{-1}. With our experimental conditions (the probe beam diameter of 40 μm, the repetition rate of 2 kHz, and the pulse duration of 3.2 ps), these power densities correspond to the average laser power of 0.05 to 2.5 mW.

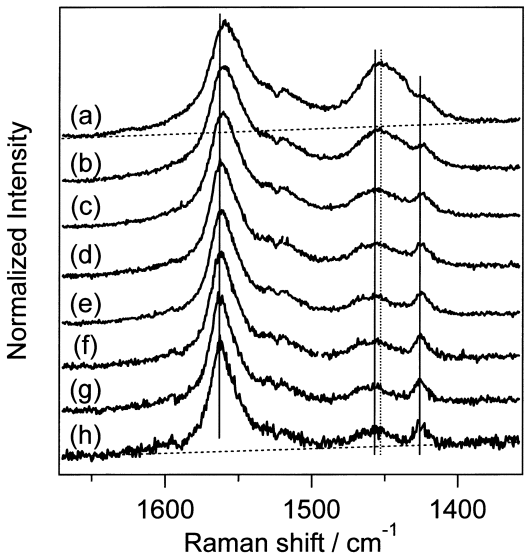

Fig. 6. Probe power dependence of the Stokes Raman bands of S_1 *trans*-stilbene measured in heptane at $t = 50$ ps. The Raman bands from S_1 *trans*-stilbene at 1570 cm^{-1}, 1457 cm^{-1}, and 1426 cm^{-1} are indicated by solid vertical lines while the solvent band at 1453 cm^{-1} is indicated by a dotted line. The probe power density was 260 GW cm^{-2} (a), 120 GW cm^{-2} (b), 81 GW cm^{-2} (c), 41 GW cm^{-2} (d), 26 GW cm^{-2} (e), 12 GW cm^{-2} (f), 8.1 GW cm^{-2} (g), and 4.1 GW cm^{-2} (h).

In time-resolved or stationary resonance Raman measurements, the obtained signal intensity is determined by the average probe power, regardless of the repetition rate. It is noteworthy that the probe light power of 2.5 mW is not large at all in standard resonance Raman measurements. Even larger laser power is commonly used. Still, the probe laser power of 2.5 mW is large enough to cause a wavenumber shift of a Raman band by 2 cm^{-1}. This is the reason why we have been using the probe power of 0.1 mW for measuring the picosecond time-resolved Raman spectra of S_1 *trans*-stilbene. Because the peak power density of an amplified picosecond or sub-picosecond laser pulse can easily exceed 10 GW cm^{-2}, laser power dependence should be examined carefully when measuring picosecond time-resolved Raman spectra. This is particularly the case when a peak shift of a few wavenumbers has a significant meaning.

Similar power dependence was also observed for other spectral regions. Transient Raman spectra of S_1 *trans*-stilbene measured with various probe power densities are shown in Fig. 6 for the spectral region of 1350 to 1650 cm^{-1}. The time delay was fixed at 50 ps. An intense Raman band at 1570 cm^{-1}, indicated with a solid vertical line, has been assigned to the central C=C stretch of S_1 *trans*-stilbene. The Raman bands at 1457 cm^{-1} and 1426 cm^{-1} are also from S_1 *trans*-stilbene. Although chloroform was used as solvent for all the other spectral data presented in this article, heptane was selected for this measurement. This is because heptane has a Raman band at 1453 cm^{-1}, as shown in the figure with a dotted line, which can be used as a good internal intensity standard. In this spectral region, there is no good solvent band available from chloroform. As the probe power density is changed from 260 GW cm^{-2} (Fig. 6a)

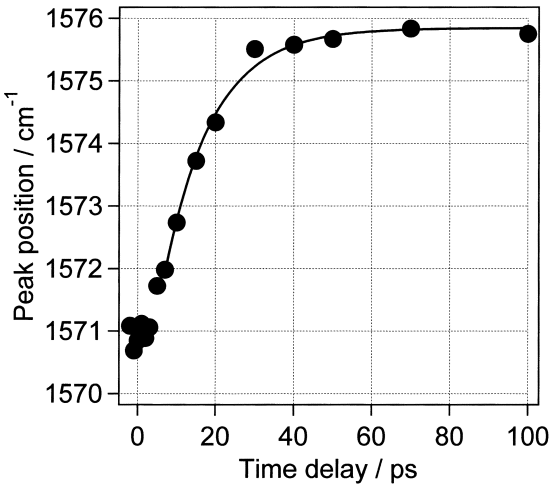

Fig. 7. Time dependence of the peak positions of the 1570 cm^{-1} Raman band of S_1 *trans*-stilbene measured in chloroform. The best fit of the peak position after 7 ps with a single exponential decay function is also shown with a solid curve. The best fit was obtained when the decay time constant was 12 ps.

to 4.1 GW cm^{-2} (Fig. 6h), the width of the 1570 cm^{-1} band from S_1 *trans*-stilbene is decreased whereas its peak position is shifted to the higher wavenumber direction.

The relative intensity ratio of the 1570 cm^{-1} band to the solvent band at 1453 cm^{-1} is decreased by a factor of 5 or more in Fig. 6 when the probe power density is increased. A possible reason for this large intensity change is depletion of the S_1 state due to effective optical pumping from the S_1 state to the S_n state caused by strong probe light field. After complete saturation of the S_n–S_1 transition, however, the S_n state should have a population equal to that of the S_1 state. This mechanism does not fully account for the observed large change of the relative intensity. It is likely that the S_1 population is lost in a sub-picosecond time scale because the S_n state is converted to other states than the S_1 state very rapidly, well within the duration of the probe pulse.

The peak positions of several Stokes scattering bands of S_1 *trans*-stilbene change depending on the time delay,[14–16] as mentioned above. This temporal shift is caused by the cooling of S_1 *trans*-stilbene to which excess vibrational energy has been given upon the photoexcitation from the ground state. An example of the peak shift measured for the central C=C stretch band in chloroform is shown in Fig. 7, where the observed peak position is plotted against time delay. As the time delay increases, the peak position changes by as large as 5 cm^{-1}. Although the cooling kinetics is well explained by the solution of the macroscopic diffusion equation of heat,[17] it is convenient to assume a single exponential decay when evaluating the cooling rate. The least squares fitting analysis with the single exponential decay function shows that the time constant for the cooling process is 12 ps.

Symmetric Component and Anti-Symmetric Component. It is possible that the observed temporal shift of the peak position of the 285 cm^{-1} band, shown in Fig. 3, includes contribution from the vibrational cooling process as well as the effect of the pump light field. We try to extract the two independent effects, vibrational cooling and pump field interference, from the obtained data. For this purpose, recorded positions of the Stokes and anti-Stokes scattering Raman bands, $\tilde{\nu}_S$ and $\tilde{\nu}_{aS}$, are converted to a new pair of variables: the symmetric component $\tilde{\nu}_{symm}$ and the anti-symmetric component $\tilde{\nu}_{anti\text{-}symm}$. These new variables are defined as

$$\tilde{\nu}_{symm} = \frac{1}{2}(|\tilde{\nu}_S| + |\tilde{\nu}_{aS}|) \quad (1)$$

$$\tilde{\nu}_{anti\text{-}symm} = \frac{1}{2}(|\tilde{\nu}_S| - |\tilde{\nu}_{aS}|). \quad (2)$$

In Eqs. 1 and 2, $|\tilde{\nu}_S|$ or $|\tilde{\nu}_{aS}|$ represents the absolute value of the Raman shift for the Stokes or anti-Stokes scattering band, that is, the distance between the Stokes or anti-Stokes Raman scattering band and the Rayleigh scattering band on the wavenumber axis.

The symmetric component, $\tilde{\nu}_{symm}$, is equal to half the energy difference between the anti-Stokes scattering band and the Stokes scattering band. It gives the intrinsic energy spacing between the vibrational levels associated with the Raman process. The anti-symmetric component, $\tilde{\nu}_{anti\text{-}symm}$, indicates the relative position of the apparent excitation energy for the observed pair of the Stokes and anti-Stokes Raman scattering bands. This value becomes zero if the Raman shift for the Stokes scattering band is equal to that for the anti-Stokes scattering band, which is considered to be true for most of the measurements. By converting a pair of $\tilde{\nu}_S$ and $\tilde{\nu}_{aS}$ to a new pair of $\tilde{\nu}_{symm}$ and $\tilde{\nu}_{anti\text{-}symm}$, we can extract the "true" energy spacing for the vibrational transition and the "apparent" excitation energy from the observed data.

The time dependence of the positions of the Stokes scattering band and the anti-Stokes scattering band at 285 cm^{-1}, once shown in Fig. 3, is converted to the symmetric and anti-symmetric components, $\tilde{\nu}_{symm}$ and $\tilde{\nu}_{anti\text{-}symm}$. The results are shown in Fig. 8. In the figure, $\tilde{\nu}_{symm}$ for three different probe power densities ((a), (b), and (c)) and the averaged values of the three (d) are plotted. Within the experimental uncertainties, no difference was observed among the $\tilde{\nu}_{symm}$ values for three probe power densities. The symmetric component, or intrinsic Raman transition energy, does not depend on the probe power density. The least squares analysis of the averaged $\tilde{\nu}_{symm}$ values revealed that their time dependence between 7 ps and 50 ps was well explained by a single exponential decay function with a time constant of 12 ps. The obtained time constant matches the one already obtained by the analysis of the 1570 cm^{-1} Stokes band (Fig. 7), which reflects the cooling process of S_1 *trans*-stilbene. Without calculating the symmetric component, it would not have been possible to extract the temporal behavior corresponding to the cooling process from the observed peak shift of the 285 cm^{-1} band.

The anti-symmetric component, $\tilde{\nu}_{anti\text{-}symm}$, indicates the apparent position of the excitation light. In Fig. 8, the $\tilde{\nu}_{anti\text{-}symm}$ value for the probe power density of 43 GW cm^{-2} is plotted in trace (e). With this power density, the time dependent change of $\tilde{\nu}_{anti\text{-}symm}$ appears most distinguished. The plot starts from 0.5 cm^{-1} at -2 ps and shows a steep decrease until 10 ps when the $\tilde{\nu}_{anti\text{-}symm}$ value reaches a stationary value at -1.7 cm^{-1}.

The symmetric and anti-symmetric components of the 261

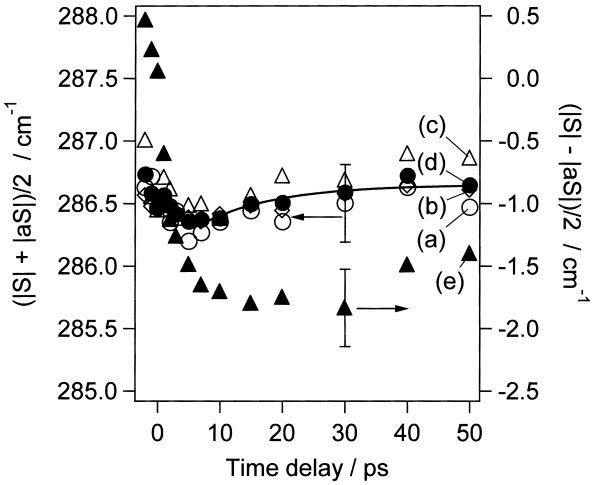

Fig. 8. Time dependence of the symmetric component $\tilde{\nu}_{\text{symm}}$ (left axis) and anti-symmetric component $\tilde{\nu}_{\text{anti-symm}}$ (right axis) of the 285 cm^{-1} band of S_1 *trans*-stilbene in chloroform. The probe power density for the symmetric component was 31 GW cm^{-2} (a), 12 GW cm^{-2} (b), and 7.4 GW cm^{-2} (c). Values of the symmetric component averaged for the three probe power densities are shown in (d). The anti-symmetric component is plotted only for the probe power density of 31 GW cm^{-2} (e). The best fit of the averaged symmetric component after 7 ps with a single exponential decay function is also shown with a solid curve. The best fit was obtained when the decay time constant was 12 ps.

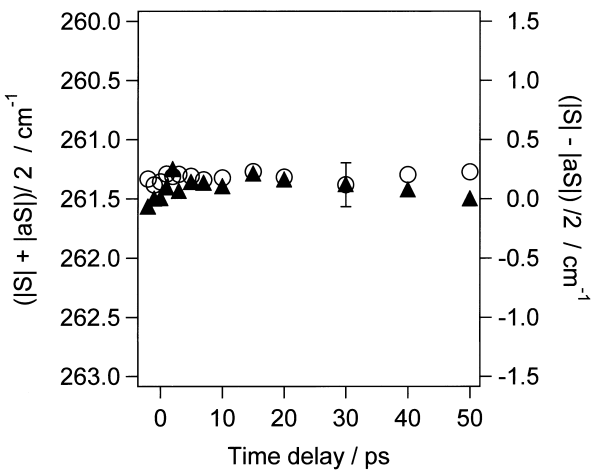

Fig. 9. Time dependence of the symmetric component $\tilde{\nu}_{\text{symm}}$ (open circles, left axis) and anti-symmetric component $\tilde{\nu}_{\text{anti-symm}}$ (filled triangle, right axis) of the 261 cm^{-1} band of chloroform. The probe power density was 31 GW cm^{-2}.

cm^{-1} band from the solvent chloroform are also calculated. Their time dependence is shown in Fig. 9. The probe power density for the measurement was 43 GW cm^{-2}, the same value as that for Fig. 8(a) and Fig. 8(e). Unlike the S_1 *trans*-stilbene Raman band, however, the $\tilde{\nu}_{\text{symm}}$ value (open circle) or the $\tilde{\nu}_{\text{anti-symm}}$ value (filled triangle) of the chloroform band shows little change. Within the experimental uncertainties, the anti-symmetric component shows a constant value with or without

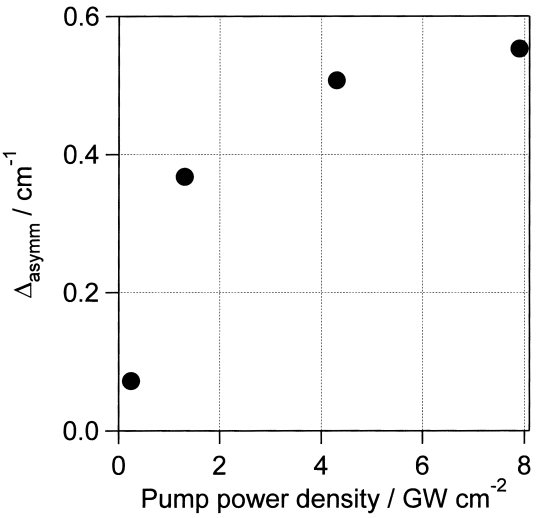

Fig. 10. Dependence of the temporal shift of the anti-symmetric component of the 285 cm^{-1} band of S_1 *trans*-stilbene on the pump power density. See text for the evaluation of the shift.

the presence of the pump light field. Its value is 0 cm^{-1}, showing no apparent change of the excitation energy. The Raman shift for the Stokes scattering band is equal to that for the anti-Stokes scattering band. The results shown in Fig. 9 confirm the conclusion that the solvent Raman bands are not affected by the pump or probe light. Time and probe power dependence observed for the S_1 *trans*-stilbene Raman band is not the result of a trivial error in wavenumber calibration.

The effect of the pump laser field was examined by analyzing the $\tilde{\nu}_{\text{anti-symm}}$ values. Difference between the averaged $\tilde{\nu}_{\text{anti-symm}}$ value for the time delays of -1, 0, 1, and 2 ps and that for 7, 10, 15, and 20 ps, Δ_{asymm}, is plotted against the pump power density in Fig. 10. The value becomes positive if $\tilde{\nu}_{\text{anti-symm}}$ is larger for smaller time delays. Because the pump pulse and the probe pulse are temporally overlapped from -1 to 2 ps, and because they are not overlapped at 7 ps or later, the Δ_{asymm} value shows the effect of the pump laser field on the apparent excitation energy. The Δ_{asymm} value converges on zero when the pump power density approaches zero. It increases as the power density increases, and reaches a value of 0.55 cm^{-1} at the power density of 8 GW cm^{-2}. For the temporal region when the pump and probe light pulses are overlapped with each other, the apparent excitation energy depends not only on the probe power density, but also on the pump power density.

Because the molar extinction coefficient of the S_1–S_0 transition of *trans*-stilbene at 294 nm is 3.1×10^4 dm^3/mol cm, which corresponds to the cross section of 5.2×10^{-17} cm^2, the excitation rate estimated for the pump power density of 8 GW cm^{-2} is 6.2×10^{11} s^{-1}. It takes 1.6 ps for a *trans*-stilbene molecule to be excited to the S_1 state under this condition of photoexcitation.

As shown in Fig. 10, the $\tilde{\nu}_{\text{anti-symm}}$ value increases when the pump power density increases. The value, however, decreases when the probe power density increases. The direction of the power dependent peak shift caused by the pump pulse is opposite to that caused by the probe pulse.

Possible Mechanisms. The effect of off-resonant light

field on an optical transition is generally described by the optical Stark effect. The optical Stark effect is formulated by the second-order perturbation on energy eigenstates caused by the interaction between the transition dipole and the external light field[1] or by the third order non-linear susceptibility commonly used in non-linear optics.[2] Observed spectral changes in rotational or vibrational bands caused by intense probe light have been explained by the optical Stark effect in stimulated Raman spectroscopy,[28,29] inverse Raman spectroscopy,[30] and CARS.[31,32] In our experimental conditions, however, the probe light is in resonance with the S_n–S_1 transition of *trans*-stilbene. The standard optical Stark effect is not applicable for the observed probe power dependence.

Deformation of the spontaneous resonance Raman bands under arbitrary probe light field was simulated by non-perturbative methods.[5,6] Correlation functions responsible for the band shapes of various optical processes involving spontaneous resonance Raman scattering were estimated by calculating the time evolution of the density operator, or by solving the Liouville equation. The polarization for the emission process is modulated by the Rabi frequency as well as the incoming probe electric field, which splits or broadens the observed Raman bands. The correlation between the Stokes scattering peak position and the anti-Stokes scattering peak position, however, has not been shown explicitly yet. The effect of the pump light field was not explained by this treatment, either.

The pump light in this study is not in resonance with the Raman process. It is possible that the optical Stark effect from the pump light affects the observed Raman signals. Becker et al. reported the deformation of the ground state absorption band of rhodamine B caused by the optical Stark effect from the off-resonant intense "pump" pulse.[3] The difficulty of the optical Stark effect in explaining the results obtained in this study is that the pump light field deforms only the Raman bands from S_1 *trans*-stilbene. It does not affect the solvent Raman bands. The ordinary formalism of the optical Stark effect derived for a two-level system does not explain the disagreement between the positions of the Stokes Raman scattering band and the anti-Stokes scattering band, either. The optical Stark effect, in the simplest form, does not explain either the probe power dependence or pump power dependence of the observed Raman spectra in the present study.

The effect of the laser field on stimulated Raman spectra has been investigated by Zinth and Kaiser.[33] Strong laser light can become positively chirped because of the self-phase-modulation at glass optics and at the sample solution. The stimulated Raman signal can also become chirped through the term $\chi^{(3)}E_LE_L{}^*E_R$, where E_L and E_R are the electric fields for the laser input and the stimulated Raman light (crossfield modulation). Because the stimulated Raman signal builds up at the later part of the input light pulse, the observed Stokes scattering band is up-shifted in absolute wavenumber, or down-shifted in Raman shift. Although we employ the 90 degree scattering geometry for the signal collection, it is possible that the observed spectra include contribution from the scattered light of stimulated Raman light as well as spontaneous Raman signals.[34] This mechanism can explain the observed up-shift of the Stokes and anti-Stokes Raman scattering bands in absolute wavenumber when the power of the probe light is increased. For solvent bands, the chirped probe pulse does not cause the wavenumber shift if they do not have contribution from the stimulated Raman process. However, there are some difficulties when applying this mechanism to the present study. The spectrum of the probe laser from the sample, as we recorded as the Rayleigh line, did not show the splitting or broadening expected as the result of self-phase-modulation (data not shown). Also, the width of the detected Raman bands was increased when the probe power was increased (Fig. 4). If the contribution from the stimulated Raman signal is increased as the probe power is increased, the bandwidth can become narrower, but not wider, than the spontaneous Raman signals.[35] It is not likely that this mechanism explains the observed effect of the pump light field. For the time region where the pump and probe pulses are temporally overlapped, the population of the S_1 state is still growing within the duration of the probe pulse. Because the stimulated Raman signals have even more contribution from the rear part of the probe light than later time delays when the S_1 population level can be regarded as constant throughout the duration of the probe pulse, the Stokes scattering band and the anti-Stokes scattering bands will move to the higher wavenumber direction, as opposed to the experimental observation.

It seems possible to explain the pump and probe power dependence of the observed Raman bands from S_1 *trans*-stilbene, if we assume that the probe light pulse is negatively chirped and that the probe light field causes the effective depletion of the S_1 state.[36] In a negatively chirped light pulse, the wavelength is shorter at the front edge of the pulse. At the beginning, the excitation energy for the Raman scattering is larger. If the probe power density is large, the probe light depletes the S_1 state quickly. When the central part of the probe pulse arrives, there is no more S_1 state left in the laser spot. The Raman spectrum of the S_1 state is measured only with the larger excitation energy. This causes the apparent shift of the excitation energy to the higher wavenumber direction, or the down-shift of the $\tilde{\nu}_{\text{anti-symm}}$ value, which agrees with the observation. The pump power dependence can be explained in a similar way. For negative time delays of a few picoseconds, the S_1 population is generated only in the rear part of the probe pulse where there is a temporal overlap with the pump. In the rear part of a negatively chirped pulse, the wavelength is longer, which results in the lower excitation energy for the Raman transition. This explains the observed positive shift of the $\tilde{\nu}_{\text{anti-symm}}$ value when the pump power is increased (Fig. 10).

The results shown in Fig. 6 mean that the second assumption for the mechanism presented in the previous paragraph, the rapid depletion of the S_1 state by the probe light, is fulfilled, at least qualitatively. The relative population of the S_1 state is decreased by a factor of 5 or more when the probe power density is increased from 4.1 to 260 GW cm^{-2}. However, the validity of the first assumption, a negative chirp in the probe pulse, is not clear. It has been confirmed that our probe light pulse is close to the Fourier transform limit. Its time-energy product, when assuming a sech^2 pulse shape, is 11.2 ps cm^{-1}, while the value for the ideal Fourier transform limited pulse is 10.5 ps cm^{-1}. If the power dependent peak shift of 2.5 cm^{-1} is caused by this mechanism, there should be a chirp of 2.5 cm^{-1} or larger for an almost Fourier transform limited

pulse of 3.5 cm^{-1}. This situation is fulfilled if the chirp is present only at the front and rear wings of the probe light pulse and if the main part of the pulse is chirp-free. In this case, a negative chirp as large as 2 cm^{-1} may not appear when analyzing the light pulse. The depletion of the S_1 state by the probe light, however, should be effective enough that the Raman spectrum is measured only by the wing part of the probe pulse. Determination of the cross section of the S_n–S_1 transition of *trans*-stilbene will allow quantitative estimation of the depletion rate of the S_1 state, which is needed for clarifying the chirp structure required for this mechanism.

Concluding Remarks

From the present study, it is obvious that the Stokes and anti-Stokes peak positions strongly depend on the pump and probe power densities, although the exact mechanism has not been clarified yet. Careful examination of the pump and probe power dependence is essential when interpreting the time-resolved resonance Raman spectra, especially for the time region where the pump and probe pulses are temporary overlapped. It is safer to set the experimental conditions so that the pump and probe pulses would not saturate the S_1–S_0 and S_n–S_1 transitions for avoiding the undesired anomalous effects reported in this article.

The author thanks Prof. H. Hamaguchi, Dr. P. Matousek, and Prof. W. Zinth for their valuable discussion. The experimental part of this work has been performed at Kanagawa Academy of Science and Technology. This work is partially supported by The Kurata Foundation and by a Grant-in-Aid for Scientific Research (B) (No. 12440158) from Japan Society for the Promotion of Science.

References

1 A. M. Bonch-Bruevich and V. A. Khodovoi, *Usp. Fiz. Nauk.*, **93**, 71 (1967); *Sov. Phys. Usp.*, **10**, 637 (1968).
2 M. Joffre, D. Hulin, A. Migus, and A. Antonetti, *J. Mod. Optic.*, **35**, 1951 (1988).
3 P. C. Becker, R. L. Fork, C. H. Brito Cruz, J. P. Gordon, and C. V. Shank, *Phys. Rev. Lett.*, **60**, 2432 (1988).
4 H. Hamaguchi, *J. Chem. Phys.*, **89**, 2587 (1988).
5 S. Mukamel, D. Gimbert, and Y. Rabin, *Phys. Rev. A*, **26**, 341 (1982).
6 B. Dick and R. M. Hochstrasser, *J. Chem. Phys.*, **81**, 2897 (1984).
7 K. Iwata and H. Hamaguchi, *J. Raman Spectrosc.*, **25**, 615 (1994).
8 R. M. Hochstrasser, *Pure Appl. Chem.*, **52**, 2683 (1980).
9 D. H. Waldeck, *Chem. Rev.*, **91**, 415 (1991).
10 H. Hamaguchi, *Vib. Spectra Struct.*, **16**, 227 (1987).
11 H. Hamaguchi and T. L. Gustafson, *Annu. Rev. Phys. Chem.*, **45**, 593 (1994).
12 M. Tasumi, T. Urano, and H. Hamaguchi, "Time Resolved Vibrational Spectroscopy," ed by G. H. Atkinson, Gordon and Reach, New York (1987).
13 H. Hamaguchi, *Chem. Phys. Lett.*, **126**, 185 (1986).
14 W. L. Weaver, L. A. Huston, K. Iwata, and T. L. Gustafson, *J. Phys. Chem.*, **96**, 8956 (1992).
15 K. Iwata and H. Hamaguchi, *Chem. Phys. Lett.*, **196**, 462 (1992).
16 R. E. Hester, P. Matousek, J. N. Moore, A. W. Parker, W. T. Toner, and M. Towrie, *Chem. Phys. Lett.*, **208**, 471 (1993).
17 K. Iwata and H. Hamaguchi, *J. Phys. Chem. A*, **101**, 632 (1997).
18 K. Iwata and H. Hamaguchi, *J. Raman Spectrosc.*, **29**, 915 (1998).
19 P. Matousek, A. W. Parker, W. T. Toner, M. Towrie, D. L. A. de Faria, R. E. Hester, and J. N. Moore, *Chem. Phys. Lett.*, **237**, 373 (1995).
20 J. Qian, S. L. Schultz, and J. M. Jean, *Chem. Phys. Lett.*, **233**, 9 (1995).
21 S. L. Schultz, J. Qian, and J. M. Jean, *J. Phys. Chem. A*, **101**, 1000 (1997).
22 T. Nakabayashi, H. Okamoto, and M. Tasumi, *J. Phys. Chem. A*, **101**, 7189 (1997).
23 T. Nakabayashi, H. Okamoto, and M. Tasumi, *J. Phys. Chem. A*, **102**, 9686 (1998).
24 D. L. Phillips, J.-M. Rodier, and A. B. Myers, *Chem. Phys.*, **175**, 1 (1993).
25 Y. Mizutani and T. Kitagawa, *Science*, **278**, 443 (1997).
26 K. Iwata, S. Yamaguchi, and H. Hamaguchi, *Rev. Sci. Instrum.*, **64**, 2140 (1993).
27 S. Takeuchi and T. Tahara, *Chem. Phys. Lett.*, **326**, 430 (2000).
28 M. E. Mack, R. L. Carman, J. Reintjes, and N. Bloembergen, *Appl. Phys. Lett.*, **16**, 209 (1970).
29 H. Moosmüller, C. Y. She, and W. M. Huo, *Phys. Rev. A*, **40**, 6983 (1989).
30 R. L. Farrow and L. A. Rahn, *Phys. Rev. Lett.*, **48**, 395 (1982).
31 L. A. Rahn, R. L. Farrow, M. L. Koszykowski, and P. L. Mattern, *Phys. Rev. Lett.*, **45**, 620 (1980).
32 M. Pealat, M. Lefebvre, J.-P. E. Taran, and P. L. Kelley, *Phys. Rev. A*, **38**, 1948 (1988).
33 W. Zinth and W. Kaiser, *Opt. Commun.*, **32**, 507 (1980).
34 Detection of CARS signals scattered to the 90 degree direction (PCARS) has been reported. See T. Ishibashi and H. Hamaguchi, *J. Chem. Phys.*, **106**, 11 (1997).
35 A. Laubereau and W. Kaiser, *Rev. Mod. Phys.*, **50**, 607 (1978).
36 P. Matousek and A. W. Parker, private communication.